PAPER

Check for updates

Excited-state AIE material for differential recognition of toxic hair color ingredients: towards functional device applications

Shagun, [a] Deekshit Dhiman, [b] Darsi Rambabu, [c] Koen Robeyns, [c] Robin Khosla[b] and Abhimanew Dhir *[a]

We designed and synthesized an imino-linked dansyl-based molecule, **DHNB**, which exhibits interactions with the hair color ingredient *p*-phenylenediamine (PPD) and its oxidative trimer, Bandrowski's Base (BWB), over other analytes tested. Variable interactions, such as intra- and inter-molecular hydrogen bonding and environment-responsive conformational dynamics, were observed, leading to contrasting responses amongst the most responsive analytes. **DHNB** exhibits Excited State Intramolecular Proton Transfer (ESIPT)-assisted Aggregation-Induced Emission (AIE) in MeOH : H$_2$O (10 : 90), which is utilized for the detection of hair color ingredients. The presence of BWB quenches the fluorescence emission of **DHNB** in MeOH : H$_2$O (10 : 90) at 497 nm, whereas in the presence of PPD, the emission at 497 nm is quenched, with simultaneous appearance of a new blue shifted band at 402 nm. Importantly, the successful detection of PPD in a commercial hair color sample underscores the practical applicability of **DHNB**. Furthermore, variations in the charge transport properties of **DHNB** in MeOH : H$_2$O (10 : 90) and upon interaction with BWB/PPD were observed *via* current−voltage (*I*−*V*) measurements, suggesting its strong potential as an electrical sensor device.

1. Introduction

Analyte-specific recognition is one of the main design principles of supramolecular systems used as templates for chemosensing applications.[1,2] Designing such excited-state systems becomes challenging because of the high sensitivity and selectivity of the fluorescence technique.[3,4] The task is accomplished by designing molecular building blocks inspired by various mechanistic approaches and cementing them covalently for recognition of the targeted analyte.[5,6] Few limitations of conventional excited state systems, such as aggregation-caused quenching, were self-addressed after the discovery of the phenomenon of Aggregation-Induced Emission (AIE).[7] Further, incorporation of a dual approach, *viz.*, Excited State Intramolecular Proton Transfer (ESIPT)-assisted AIE, initiated the design and synthesis of more

complex systems for recognition of different analytes of environmental and biological significance.[8,9]

In this context, our research focuses on the design and synthesis of new AIE materials for sensing applications.[10,11] Recently, we reported an AIE-active molecule for multimodal recognition of antibiotics[12] and related efforts, highlighting its potential for forensic applications.[13] In continuation of our research program to design and synthesize new AIE materials for molecular recognition, in the present study, we report a dansyl-based system, **DHNB**, which displays ESIPT-assisted AIE behavior in a MeOH : H$_2$O (10 : 90) solvent mixture. The aggregates of the system are utilized for the detection of hair color ingredients and their analogues, namely, Bandrowski's Base (BWB), *p*-phenylenediamine (PPD), *o*-phenylenediamine (OPD), *m*-phenylenediamine (MPD), hydroquinone (HQN), 2,4-diaminopyrimidine (DPM), melamine (MLN), and triphenylmethanamine (TMA) (*vide infra*).

Despite several reports of PPD detection[14–16] and its associated side effects,[17–20] many commercial hair dyes available in the market continue to use PPD as the main coloring ingredient. PPD in hair dye formulations is subjected to oxidation in the presence of an oxidizing agent, generally H$_2$O$_2$, before being applied to the scalp, forming a trimeric oxidized product, *i.e.*, Bandrowski's base (BWB), through a free radical reaction pathway.[21] Though few reports claim that BWB is less toxic than PPD because of its higher molecular weight and limited epidermal

a School of Chemical Sciences, Indian Institute of Technology Mandi, Kamand, Himachal Pradesh-175005, India. E-mail: shagungorsi@gmail.com, abhimanew@iitmandi.ac.in

b School of Computing and Electrical Engineering, Indian Institute of Technology Mandi, Kamand, Himachal Pradesh-175005, India. E-mail: d23261@students.iitmandi.ac.in, robin@iitmandi.ac.in

c Institute of Condensed Matter and Nanosciences, Molecular Chemistry, Materials and Catalysis, Université catholique de Louvain, Louvain-la-Neuve B-1348, Belgium. E-mail: rambabu.darsi@uclouvain.be, koen.robeyns@uclouvain.be

Paper   **Journal of Materials Chemistry C**
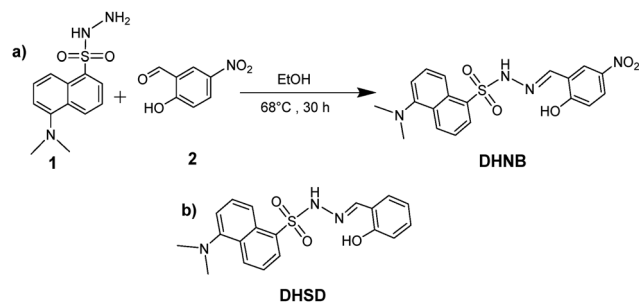
Fig. 1 (a) Synthetic route of compound **DHNB**; and (b) reference compound **DHSD**.
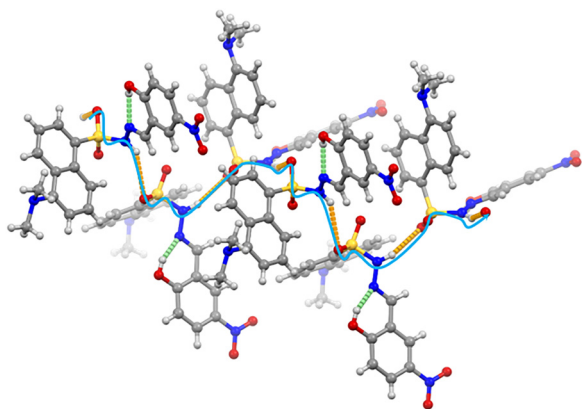

Fig. 2 X-ray structure of **DHNB**, highlighting two types of hydrogen bonding interactions: intramolecular hydrogen bonding (shown in light green) and intermolecular hydrogen bonding (shown in orange), forming a chain-like arrangement (blue).

penetration,[22,23] the extent of PPD conversion to BWB in actual formulations remains poorly quantified. There is also a possibility that PPD and BWB can coexist when the consumer uses the hair dye formulation. PPD is known to cause allergic dermatitis,[20] and the role of BWB is speculative, although reports claim that the PPD only acts as a prohapten and is transformed into BWB, which acts as a hapten and is the main cause of skin allergies.[24,25] Thus, the role of BWB as an allergen cannot be ruled out. Different fluorescent probes for PPD detection are listed in Table S1 of the SI. Within the limits of our information, optical sensors for BWB are not available in the literature.

Herein, we show that **DHNB** (Fig. 1a and 2) exhibits ESIPT-assisted AIE behavior facilitated by the modulation of its orientation (*vide infra*). The aggregates of **DHNB** show a contrasting fluorescence behavior towards both analytes (BWB and PPD). The increased global use of hair dyes in recent years[26] underscores the need for reliable detection of components such as BWB and PPD. Thus, developing a single probe capable of a contrasting mode detection for both compounds is highly significant. To the best of our knowledge, a fluorescent chemosensor for BWB and a chemosensor that can differentiate between BWB and PPD in a contrasting manner are unprecedented in the literature. Keeping in view the significance of the work, we further explored the *I–V* behavior of the native molecule as aggregates in the presence and absence of both

of the above-mentioned analytes to establish its potential for the development of an electrical sensor device.[27,28]

2. Experimental section

2.1. Materials and instrumentation

All commercially available chemicals and analytical-grade solvents were purchased from reliable suppliers and used without further purification. The commercial hair color utilized for the study was purchased from a local market. ^{1}H and ^{13}C NMR spectra were recorded on a JEOL ECX 500 MHz spectrometer with TMS as internal standard. Mass spectrometry was performed using an HRMS Bruker Impact HD. Single-crystal X-ray data were collected on a monochromated (multilayer optics) dual-source (Cu and Mo) Bruker D8 Venture, equipped with an Eos CCD detector, using MoKα ($\lambda = 0.71073$) at 171 K. Data acquisition, reduction and multi-scan absorption correction were performed with the Bruker Apex4 suite. The structure was solved by SHELXT and refined by SHELXL2019/3. Ultraviolet-visible absorbance spectra were recorded on a UV-visible spectro-photometer (Shimadzu UV-2450), and fluorescence studies were performed using an Agilent fluorescence spectrometer (Cary Eclipse). Fluorescence lifetime measurements were performed using a Delta Flex TCSPC system (Horiba Scientific), with pulsed LED sources. DLS was performed on a Zetasizer Nano ZS from Malvern Instruments Ltd. Scanning electron microscopy (FE-SEM, ZEISS, Gemini SEM 500) and transmission electron microscopy (HR-TEM, Thermo Fisher, Tecnai G2 20 S-TWIN) were used for microscopic imaging. For the fabrication of sensor devices, Ti/Pt micro-interdigitated electrodes (IDE) were fabricated using DC magnetron sputtering on cleaned (acetone, IPA and DI ultrasonicated) glass substrates, followed by deposition of the sensor thin film by spin coating at 3000 rpm for 30 s. The current–voltage (*I–V*) characteristics were measured using a Keithley SCS 4200 system.

2.2. Synthesis of probe DHNB, reference compound DHSD and analyte Bandrowski's base BWB

Synthesis of 5-(dimethylamino)-N'-(2-hydroxy-5-nitrobenzylidene)-naphthalene-1-sulfono hydrazide (DHNB): ethanolic solutions of dansyl hydrazine (1) (30 mg, 0.11 mmol) and 2-hydroxy-5-nitrobenzaldehyde (2) (18.9 mg, 0.11 mmol) were refluxed for 30 h (Fig. 1a). The completion of the reaction was marked by color change of the yellow colored reaction mixture to dark pink. The product was recrystallised and collected from ethanol (yield = 89%); mp: 190 °C; ^{1}H NMR (500 MHz, CDCl$_3$) δ 10.81 (s, 1H), 8.94 (s, 1H), 8.62 (d, $J = 8.4$ Hz, 1H), 8.42 (d, $J = 7.5$ Hz, 1H), 8.35 (d, $J = 8.4$ Hz, 1H), 8.08 (dd, $J = 9.1, 2.7$ Hz, 1H), 7.98 (d, $J = 2.7$ Hz, 1H), 7.90 (s, 1H), 7.60 (td, $J = 8.3, 2.6$ Hz, 2H), 7.20 (d, $J = 7.3$ Hz, 1H), 6.92 (d, $J = 9.3$ Hz, 1H), 2.88 (s, 6H); ^{13}C NMR (125 MHz, CDCl$_3$) δ 163.01 (s), 148.02 (s), 140.39 (s), 131.76–131.36 (m), 129.26 (s), 127.21 (s), 126.79 (s), 123.51 (s), 117.92 (s), 115.72 (s), 45.52 (s) (Fig. S1 and S2); HRMS found [M + H]$^+$: 415.1184 (Fig. S3). Crystals were obtained by slow evaporation of

DHNB in DCM : hexane (1 : 2) solution. Crystal data for DHNB is available at CCDC number: 2480993. (Fig. S4).

The reference compound DHSD (Fig. 1b) was synthesized by following the reported procedure.[29] Analyte BWB was also synthesized from PPD.[30]

3. Results and discussion

3.1. Single-crystal X-ray diffraction of DHNB

The structure of DHNB was confirmed by single-crystal X-ray diffraction (SCXRD), in addition to NMR and mass spectrometry. DHNB crystallizes in the trigonal space group $R\bar{3}$ and comprises two distinct subunits: the dansyl moiety and the 2-hydroxy-5-nitrobenzaldehyde fragment, connected via an imine linkage (Fig. S4). These subunits exist in two different planes, linked via a sulfur atom, where S1–N4–N5 has a bond angle of 115.81° (Fig. S4 and S5), resulting in a V-shaped arrangement. The dansyl moiety is found disordered and was refined over 2 sites (64/36 ratio). Further, we observed that the three molecular units are arranged in a particular fashion, with the naphthyl rings of these three dansyl units lying in three different planes at an angle of 82.42° (Fig. S4 and S5).

DHNB exhibits two types of hydrogen bonding interactions. The first one is an intramolecular hydrogen bond between the hydroxyl (O16) hydrogen and the imino nitrogen (N5) (O–H···N), (Fig. 2 and Table S3). The second type is an intermolecular hydrogen bond between the oxygen (O2) of the sulfonyl group in one DHNB molecule and the –NH proton of an adjacent DHNB molecule (N–H···O), extending into a 1D chain-like twisted array along the c-axis (Fig. 2 and Table S3). Along these hydrogen-bonding interactions, additional C–H···π interactions occur between the naphthalene rings of different molecules (Fig. S6). Furthermore, parallel displaced π···π stacking interactions are observed between the naphthalene moieties and the 2-hydroxy-5-nitrobenzaldehyde units (Fig. S6). The overall structure forms a hexagonal arrangement, with hydrophobic N-methyl groups positioned inside the hexagonal core within the assembly (Fig. S7).

3.2. Photophysical properties of DHNB

Investigation of the solvent sensitivity of the designed donor–acceptor system DHNB revealed its diverse fluorescence response in different solvent media. While going from non-polar solvents to polar solvents, the sharp emission peaks in the fluorescence spectra of DHNB (5.0 μM) around 400 nm, 430 nm and 450 nm, respectively, in n-hexane, chloroform (CHCl₃) and dichloromethane (DCM) became broader and red shifted in tetrahydrofuran (THF) and ethyl acetate (EtOAc) and eventually disappeared in ethanol (EtOH), methanol (MeOH) and deionized water (H₂O), showing only one broad emission peak aided with significant red shift, with rise in solvent polarity (Fig. S8). It can be speculated that sharp emission peaks of DHNB in non-polar solvents, where intramolecular hydrogen bonding may be strong, arise from the facilitation of excited-state intramolecular proton transfer (ESIPT) phenomena due to stabilization of the

proton-transferred excited state, along with locally excited (LE) states.[31] In addition, the synergistic effect of ESIPT and intermolecular hydrogen bonding gives rise to a charge transfer (CT) state, through enhancement of conformational changes in DHNB, accompanied by distortion within the molecule, emerging as a red shifted band in the emission spectra.[32] However, we hypothesized that in the presence of polar protic environments, DHNB undergoes inhibition of ESIPT phenomenon because of interference from solvent protons, leading to inhibition in the formation of the six membered cyclic intermediate, which is an essential requirement for ESIPT, causing disappearance of its emission peaks and forming a charged-separated state, which appears as a red shifted single emission peak, reported to be more effectively stabilized by polar solvents.[33] Additionally, the high susceptibility of this CT state towards non-radiative decay as compared to the LE state is observed as a substantial drop in fluorescence intensity of DHNB in polar solvents.[34] We also confirmed the overall stability of DHNB with the help of NMR and fluorescence spectroscopy. The compound was found to be stable even after prolonged storage and exposure to 365 nm UV illumination (Fig. S27 and S28).

3.3. Aggregation-induced emission in DHNB

The preliminary AIE behavior of DHNB was investigated across a range of MeOH and H₂O mixtures (0% to 90%) under 365 nm UV illumination (Fig. 3a). The fluorescence spectra at all ratios were recorded, and the maximum fluorescence intensity of DHNB (5.0 μM) with emission band at 497 nm was observed in the MeOH : H₂O (10 : 90) solvent fraction (λ_{ex} = 326 nm) (Fig. 3b). To confirm the attribution of this fluorescence enhancement to the formation of aggregates, DLS, SEM and TEM studies were performed. DLS of DHNB in 100% MeOH showed an average
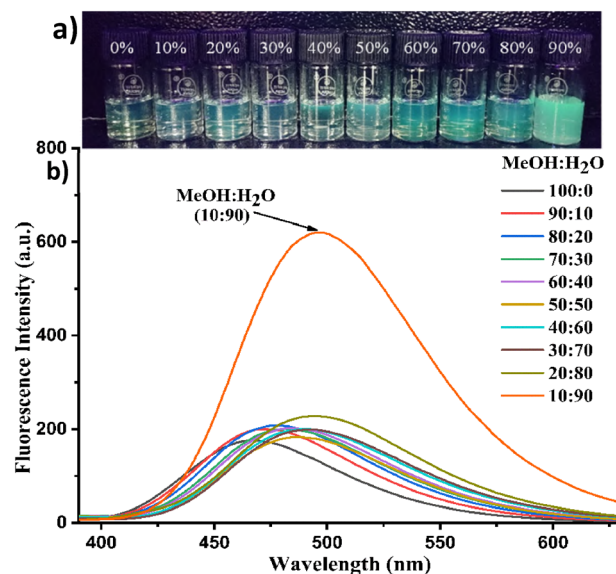

Fig. 3 (a) **DHNB** (5.0 μM) in varying % H₂O fractions in mixtures with MeOH captured under 365 nm UV illumination and (b) fluorescence emission spectra of **DHNB** (5.0 μM) in varying % H₂O fractions in mixtures with MeOH (λ_{ex} = 326 nm).

particle size of 63 nm (PDI = 0.13), whereas the DLS of DHNB in MeOH : H$_2$O (10 : 90) showed a substantial increase in particle size, indicating the possibility of aggregate formation, though with a broad size distribution range (PDI = 0.87) (Fig. S9). Further investigation through SEM and TEM revealed the presence of a self-assembled network of DHNB in MeOH : H$_2$O (10 : 90) in comparison to the dispersed particles of DHNB as observed in 100% MeOH (Fig. 4). This network can be identified as an ordered arrangement of aggregates coming together to generate J-aggregates.[35,36] The comparison of fluorescent properties of dispersed DHNB with DHNB J-aggregates showed fluorescence intensification with a quantum yield enhancement from 0.14 to 0.48. An increase in fluorescence lifetime[37,38] of DHNB was observed in MeOH : H$_2$O (10 : 90) in comparison to DHNB in 100% MeOH by a factor of 39.2% (Fig. S10). Thus, from the above discussions of ESIPT and AIE, we believe that both these mechanisms are cooperative in the DHNB excited state and are regulated by its controlled acidity due to the presence of a strong electron-withdrawing –NO$_2$ group at the *para* position to –OH, increasing its acidity and making the phenomenon of ESIPT more favorable[39,40] and consequently leading to AIE. This is because the introduction of the –NO$_2$ substituent modulates the electron-withdrawing strength and intermolecular packing, which together facilitate aggregation and stabilize the emissive charge-transfer (CT) state, accounting for the observed AIE behavior.

To confirm the role of the –NO$_2$ group in enhancing the likelihood of AIE, we synthesized a reference compound DHSD (Fig. 1b), lacking the –NO$_2$ group. No significant enhancement in intensity was observed upon exploring the AIE behavior of DHSD (Fig. S14), clearly justifying the role of –NO$_2$ in the emergence of AIE. These arguments are also well supported by the crystal structure of DHNB, where the persistence of intramolecular hydrogen bonding in its packing arrangement acts as a driving force for ESIPT, and its combined effect with intermolecular H-bonding interactions gives rise to a CT state,

as also manifested in its fluorescence behavior.[41] Therefore, DHNB in MeOH : H$_2$O (10 : 90) is utilized as a template for the detection of targeted analytes.

3.4. Fluorescence response of DHNB towards various analytes

The sensitivity of DHNB (5.0 μM) in MeOH : H$_2$O (10 : 90) was first evaluated for all the analytes, *viz.* Bandrowski's base (BWB), *p*-phenylenediamine (PPD), *o*-phenylenediamine (OPD), *m*-phenylenediamine (MPD), hydroquinone (HQN), 2,4-diaminopyrimidine (DPM), melamine (MLN), and triphenylmethanamine (TMA) (Fig. 5).

One of the most significant fluorescence changes in DHNB was observed with BWB, where it shows quenching of its emission at 497 nm upon the addition of 115.0 μM BWB (Fig. 6a). DHNB exhibited linear dependence upon an increase in the BWB concentration in the 0–60.0 μM range (R^2 = 0.99362), showing quenching
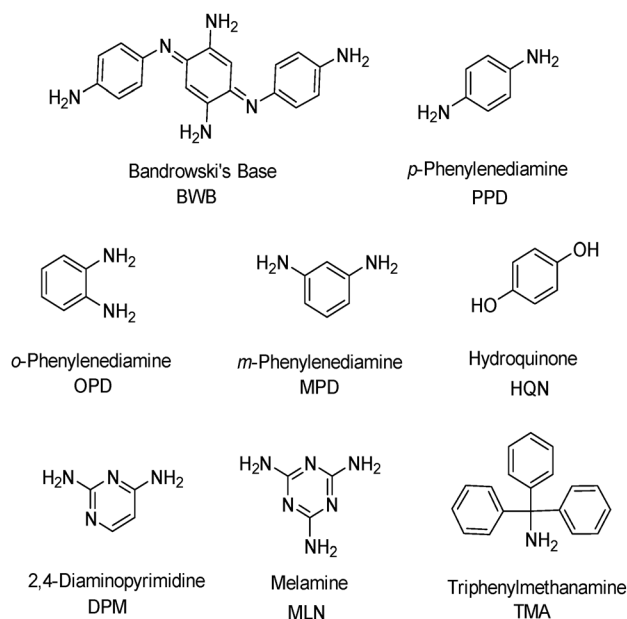
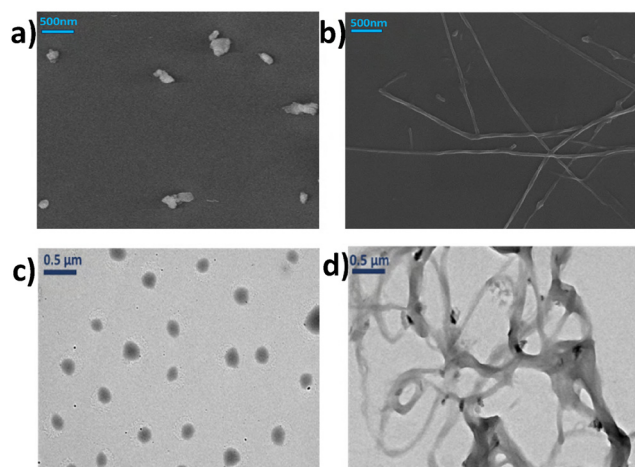**Fig. 5** Chemical structures of various analytes studied.

Fig. 4 SEM image of **DHNB** in (a) 100% MeOH and (b) MeOH : H$_2$O (10 : 90). TEM image of **DHNB** in (c) 100% MeOH and (d) MeOH : H$_2$O (10 : 90).
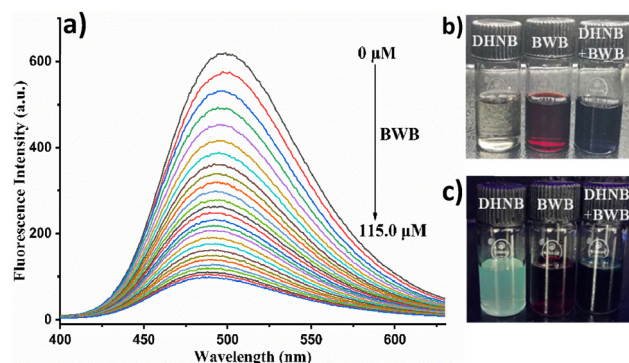
Fig. 6 (a) Fluorescence emission spectra of **DHNB** (5.0 μM) in MeOH : H$_2$O (10 : 90) upon the addition of increasing concentration of BWB (115.0 μM) (λ_{ex} = 326 nm); the solutions were observed under (b) visible light and (c) 365 nm UV illumination.
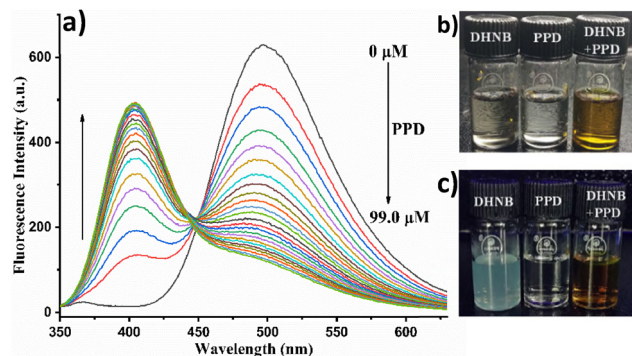
Fig. 7 (a) Fluorescence emission spectra of **DHNB** (5.0 μM) in MeOH : H$_2$O (10 : 90) upon the addition of increasing concentration of PPD (99.0 μM) (λ_{ex} = 326 nm); the solutions were observed under (b) visible light and (c) 365 nm UV illumination.
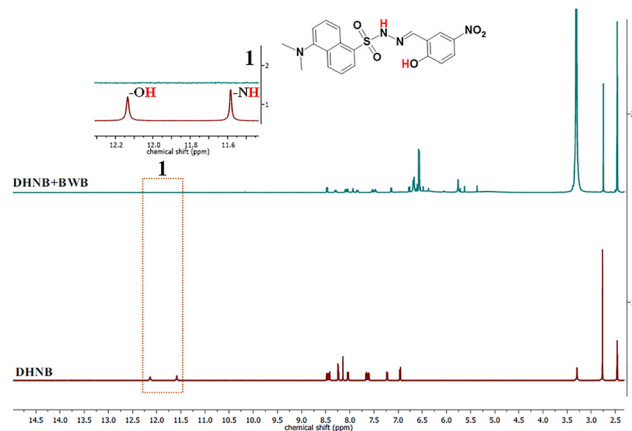

Fig. 8 Changes in the ^{1}H NMR spectra of (a) **DHNB** in DMSO-d$_6$ to (b) **DHNB** upon the addition of BWB in DMSO-d$_6$; inset 1 shows the disappearance of −OH and −NH protons of **DHNB** upon BWB addition.

efficiency, as evaluated *via* the calculation of Stern–Volmer constant, K_{SV} = 2.38 × 10^4 M^{-1} (Fig. S17) and a detection limit (LOD) of 10.2 × 10^{-6} M, displaying the sensitivity of DHNB towards BWB.

Interestingly, PPD displayed a contrasting sensing response in comparison to BWB. The emission peak of DHNB at 497 nm was quenched upon addition of 99.0 μM PPD, with a concurrent rise in the peak at 402 nm (Fig. 7a). The emission intensity of DHNB showed linear dependence upon the addition of PPD in the concentration range of 0–90.0 μM (R^2 = 0.99580), exhibiting a quenching efficiency K_{SV} = 3.63 × 10^4 M^{-1} (Fig. S18) and a detection limit (LOD) of 12.5 × 10^{-6} M.

Further, the fluorescence response of DHNB towards different analytes, including PPD analogues and derivatives, such as *o*-phenylenediamine (OPD), *m*-phenylenediamine (MPD), hydroquinone (HQN), 2,4-diaminopyrimidine (DPM), melamine (MLN), and triphenylmethanamine (TMA) (Fig. 5), was evaluated. However, none of the other analytes (99.0 μM) could elicit any significant spectral changes in DHNB (Fig. S11 and S12). The comparative behavior of BWB and PPD *vs.* other analytes was also evaluated based on changes in fluorescence intensity upon addition of the same concentration of each analyte (Fig. S13).

Additionally, the evaluation of the sensing response of the reference compound DHSD towards BWB and PPD revealed its negligible fluorescence sensing behavior towards both analytes. The concentrations of BWB (178.0 μM) and PPD (120.0 μM) required to elicit significant spectral changes in comparison to DHNB were much higher, confirming the role of the −NO$_2$ group in the efficient sensing of DHNB (Fig. S15). SEM analyses of DHSD (Fig. S16) show irregular, loosely packed aggregates. There is a possibility that this decrease in aggregated state in comparison to DHNB (Fig. 4) results in a weaker response to the analytes tested. Thus, it indicates that the improved sensitivity of DHNB arises from its more ordered aggregate morphology promoted by the −NO$_2$ group.

3.5. Sensing mechanism of BWB and PPD

The mechanism behind the detection of BWB and PPD is established by NMR titration experiments. Upon the addition of BWB to DHNB, the −NH (δ = 11.58 ppm) and −OH (δ = 12.15 ppm) proton

signals disappear (Fig. 8), indicating deprotonation. This deprotonation thus inhibits ESIPT and disrupts induced AIE, leading to the disintegration of J-aggregates, as observed through SEM (Fig. S19). This manifestation is observed in the fluorescence spectra as a quenching of the 497 nm emission AIE band of DHNB (Fig. 6a). BWB sensing can also be visually marked by the appearance of dark blue color upon the addition of a reddish-brown solution of BWB to the colorless DHNB solution (Fig. 6b).

Upon the addition of PPD to DHNB, its NMR spectra became slightly complex, which is indicative of the easy transformation of PPD into a mixture of its monomeric, dimeric, oligomeric, and polymeric oxidation products[21] (Fig. 9). The disappearance of −NH (δ = 11.58 ppm) and −OH (δ = 12.15 ppm) proton signals could be due to the interaction of DHNB with BWB (formed *in situ*) (*vide supra*) (Fig. 8). The bright yellow color of the DHNB and PPD mixture (Fig. 7b) indicates the formation of visually recognizable semi benzoquinone diamine radical cation (SBQDIRC) (Fig. S20)[21] as compared to the initially colorless PPD and DHNB solutions. SBQDIRC tends to exist in equilibrium with its non-protonated neutral form, which initiates the dye formation process during hair coloration by binding to a coupler molecule.[21] Thus, the transformation of PPD to *para*-benzoquinone diimine (BQDI) (Fig. S20) *via* a two-electron transfer through intermediate SBQDIRC suggests its inclination towards protonating electron rich *N*-dimethyl amino of the DHNB molecule, manifested as a splitting of its 6-proton singlet at δ = 2.770 ppm upon PPD addition (Fig. 9). To confirm the protonation hypothesis, fluorescence titrations were performed between DHNB in 100% MeOH with trifluoroacetic acid (TFA) (Fig. S21a), wherein a fluorescence response similar to PPD was observed, *i.e.*, quenching of emission at 497 nm and emergence of a new band at 402 nm upon the addition of increasing TFA concentrations. The formation of this species is confirmed *via* HRMS as [M + H]$^+$: 523.3175 (Fig. S21b).

3.6. Commercial hair color sample analysis

To assess the practical application of DHNB, PPD detection was tested on commercial hair color. Generally, these hair color
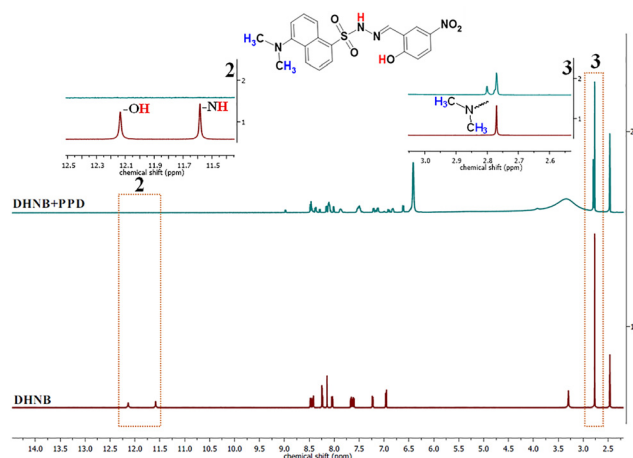
Fig. 9 Changes in the ^{1}H NMR spectra of (a) **DHNB** in DMSO to (b) **DHNB** upon the addition of PPD in DMSO-d_6; inset 2 shows the disappearance of −OH and −NH protons of **DHNB** and inset 3 shows the splitting of the N-dimethyl amino proton signal, upon PPD addition.

samples contain many potential interferents, which may hinder the performance of DHNB in detecting PPD. However, DHNB displayed an excellent sensing performance, yielding comparable results for PPD detection in the presence and absence of hair color ingredients.

100 mg of the hair color sample was prepared by mixing the colorant (CO) and developer (DE) in a 1:1 ratio for 15 min (Fig. 10a). The mixture was then dissolved in 10 ml of H_2O. The dissolution process was facilitated by sonication, followed by centrifugation and filtration. The collected supernatant, called CODE solution, exhibited the characteristic PPD peak in its fluorescence spectra (Fig. S22a) and in HRMS as $[M^+]$: 108.1604 (Fig. S22b), again corresponding to PPD. When titrated against DHNB (5.0 μM) in MeOH:H_2O (10:90), the CODE solution yielded comparable fluorescence response in DHNB (Fig. 10b), as observed for DHNB with PPD, substantiated by the appearance of dark yellow color of the final solution (Fig. 10c). The titrations of DHNB with control solutions, i.e., colorant (CO), developer (DE) (extracted via similar process mentioned for CODE) and commercially purchased resorcinol (RSN) (a major ingredient in hair colors, along with PPD) prompted no significant unexpected spectral changes in its emission (Fig. S23). Therefore, aggregates of DHNB are efficient in detecting PPD in commercial samples.

Further, to assess the influence of pH or ionic variations on the sensing behavior pertinent to real-world samples, we tested the CODE solution towards DHNB (5.0 μM) at three different pH values (pH 6.8, 7.1, and 8.2) in HEPES:MeOH (90:10, v/v). The sensing behavior remains similar at different pH values (Fig. S24).

3.7. *I–V* measurements for potential sensor device development

We assumed that the strong electron-withdrawing nature of p-nitrophenol in DHNB modulates the electronic properties of the system. Additionally, the existence of C–H$\cdots\pi$, $\pi\cdots\pi$ stacking and other intermolecular interactions in the crystal lattice of DHNB (Fig. S6) indicate its charge transport properties,[42] which
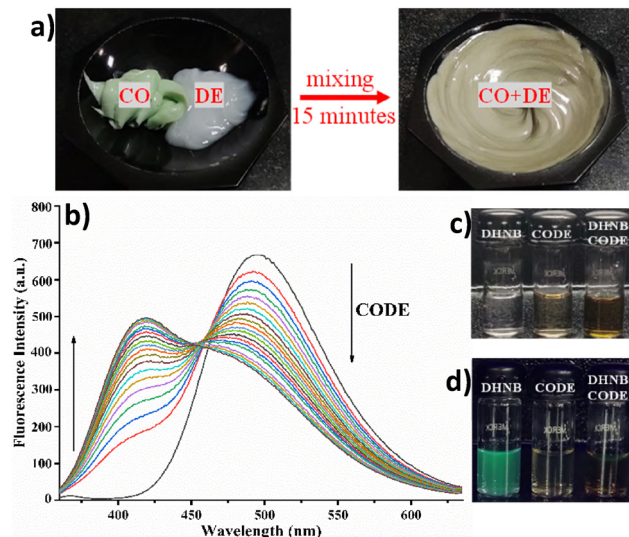

Fig. 10 (a) Mixing of colorant (CO) and developer (DE) in a 1:1 ratio. (b) Fluorescence emission spectra of **DHNB** (5.0 μM) in MeOH:H_2O (10:90) upon the addition of an increasing volume of the CODE solution (λ_{ex} = 326 nm); the solutions were observed under (c) visible light and (d) 365 nm UV illumination.

encouraged us to evaluate the electrical characteristics of the system in the presence and absence of both the analytes, i.e., BWB and PPD. The rationale for evaluating the electrical characteristics was to assess the potential of DHNB for device preparation. The *I–V* characterization was performed by sweeping the voltage between −1.0 V and +1.0 V (Fig. S25 and S26).

In the absence of any analyte, DHNB showed negligible current flow. On subsequent additions of both analytes, i.e., BWB and PPD, a concomitant increase in current is observed. The peak value of ∼6.0 nA is attained in both cases at a potential of 1.0 V, though the amount of BWB used for maximum current flow is 1.0 ppm (Fig. 11), whereas a similar amount of current flow
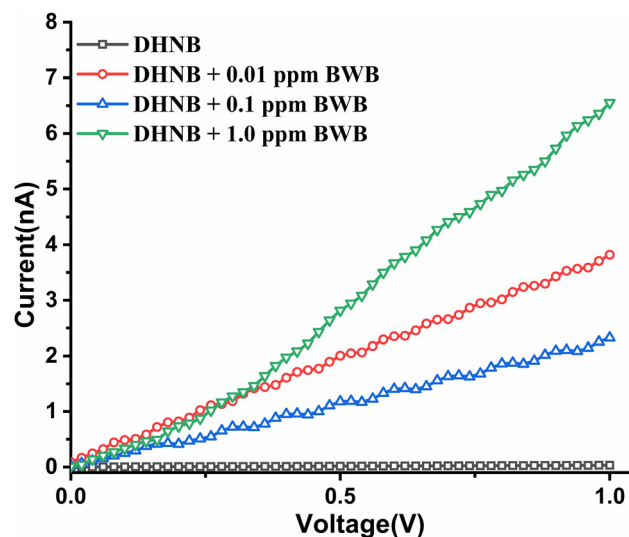

Fig. 11 *I–V* plot of **DHNB** upon the addition of an increasing concentration of BWB (1.0 ppm).
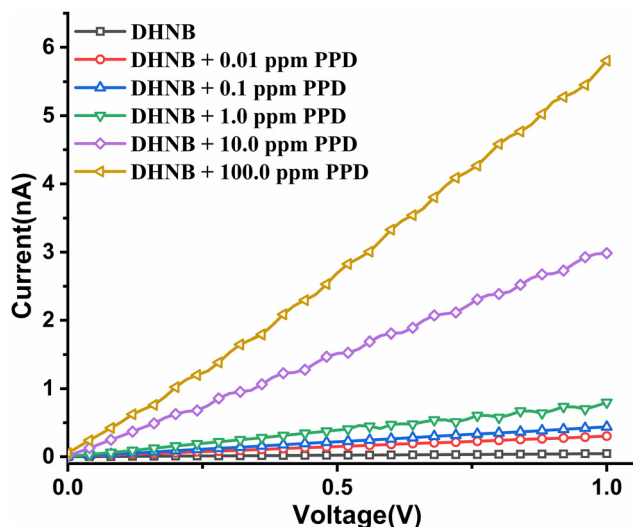
Fig. 12 *I–V* plot of **DHNB** upon the addition of an increasing concentration of PPD (100.0 ppm).

is generated on the addition of 100.0 ppm of PPD (Fig. 12). This current flow behavior supports our proposed mechanism (*vide supra*). BWB promotes the deprotonation of DHNB, resulting in a rapid current flow at lower concentrations. In the case of PPD, the stepwise formation of polymeric oxidized products and the *in situ* formation of BWB, which induces deprotonation, result in a slower rate of increase in current at higher concentrations of PPD in comparison to BWB. Thus, DHNB behaves as an n-type semiconductor in the presence of both analytes. The *I–V* studies manifest the potential of DHNB as a device for BWB and PPD sensing.

4. Conclusions

In conclusion, a new AIE material, DHNB, capable of differential detection of BWB and PPD is reported. The system is equally effective in detecting PPD in commercial samples, offering a practical solution for monitoring allergenic hair color ingredients. The *I–V* studies performed indicate its promising potential in the development of sensor devices. Selective detection of both the analytes is crucial for toxicological assessment, quality control in cosmetics, and consumer safety.

Author contributions

Shagun: investigation, methodology, data curation, writing – original draft; Deekshit Dhiman: methodology, data curation (*I–V* measurements); Darsi Rambabu and Koen Robeyns: Investigation and formal analysis (solving and analysis of single crystal X-ray structure); Robin Khosla: supervision, review and editing (*I–V* measurements); Abhimanew Dhir: conceptualization, supervision, resources, writing – review and editing.

Conflicts of interest

There are no conflicts to declare.

Data availability

The data supporting this article have been included as part of the supplementary information (SI). Supplementary information is available. See DOI: **https://doi.org/10.1039/d5tc03630e**.

CCDC 2480993 contains the supplementary crystallographic data for this paper.[43]

Acknowledgements

References

1 G. Fukuhara, *J. Photochem. Photobiol., C*, 2020, **42**, 100340.
2 T. W. Bell and N. M. Hext, *Chem. Soc. Rev.*, 2004, **33**, 589–598.
3 The measurement of sensitivity in fluorescence spectroscopy, **https://www.photonicsonline.com/doc/the-measurement-of-sensitivity-in-fluorescenc-0002**, (accessed October 3, 2025).
4 J. Sun, Y. Liu, K. Duan, Y. Shi, J. Wang, C. Deng, C. Liu and H. Xiao, *Microchem. J.*, 2025, **212**, 113322.
5 C. Guo, A. C. Sedgwick, T. Hirao and J. L. Sessler, *Coord. Chem. Rev.*, 2021, **427**, 213560.
6 Q. Lin, T. T. Lu, X. Zhu, T. B. Wei, H. Li and Y. M. Zhang, *Chem. Sci.*, 2016, **7**, 5341–5346.
7 J. Mei, N. L. C. Leung, R. T. K. Kwok, J. W. Y. Lam and B. Z. Tang, *Chem. Rev.*, 2015, **115**, 11718–11940.
8 S. Sharma, A. Dhir and C. P. Pradeep, *Sens. Actuators, B*, 2014, **191**, 445–449.
9 P. Zhou and K. Han, *Aggregate*, 2022, **3**, e160.
10 S. Sharma, C. P. Pradeep and A. Dhir, *New J. Chem.*, 2015, **39**, 1822–1826.
11 S. Sharma, C. P. Pradeep and A. Dhir, *Mater. Sci. Eng., C*, 2014, **43**, 418–423.
12 Shagun and A. Dhir, *Asian J. Org. Chem.*, 2025, **14**, e202500207.
13 M. Sharma, Shagun, A. Chhillar, A. Jaiswal and A. Dhir, *Analyst*, 2025, 1–5.
14 K. Ngamdee, S. Martwiset, T. Tuntulani and W. Ngeontae, *Sens. Actuators, B*, 2012, **173**, 682–691.
15 X. Wang, Y. Bai, Q. He, J. Li, S. Wang, W. Guo and X. Sun, *Int. J. Biol. Macromol.*, 2024, **254**, 127783.
16 J. He, J. Sunarso, J. Miao, H. Sun, J. Dai, C. Zhang, W. Zhou and Z. Shao, *J. Hazard. Mater.*, 2019, **369**, 699–706.
17 R. Shi, Z. Zhang, A. Zeb, X. Fu, X. Shi, J. Liu, J. Wang, Q. Wang, C. Chen, W. Sun and W. Liu, *Sci. Total Environ.*, 2024, **957**, 177742.
18 E. Seydi, M. Fatahi, P. Naserzadeh and J. Pourahmad, *Xenobiotica*, 2019, **49**, 1143–1148.
19 S. L. More, E. S. Fung, C. Mathis, A. M. Schulte and D. Hollins, *Regul. Toxicol. Pharmacol.*, 2023, **138**, 105331.
20 F. Hueber-Becker, G. J. Nohynek, W. J. A. Meuling, F. Benech-Kieffer and H. Toutain, *Food Chem. Toxicol.*, 2004, **42**, 1227–1236.

21 A. Meyer and K. Fischer, *Environ. Sci.: Eur.*, 2015, **27**, 1–16.

22 L. M. Pot, S. M. Scheitza, P. J. Coenraads and B. Blömeke, *Contact Dermatitis*, 2013, **68**, 193–207.

23 M. Bilal and H. M. N. Iqbal, *Sci. Total Environ.*, 2019, **670**, 555–568.

24 P. Aeby, T. Sieber, H. Beck, G. F. Gerberick and C. Goebel, *J. Invest. Dermatol.*, 2009, **129**, 99–109.

25 J. M. L. White, P. Kullavanijaya, I. Duangdeeden, R. Zazzeroni, N. J. Gilmour, D. A. Basketter and J. P. McFadden, *Clin. Exp. Allergy*, 2006, **36**, 1289–1293.

26 E. Gerstell, S. Marchessou, J. Schmidt and E. Spagnuolo, *How COVID-19 is changing the world of beauty*, 2020.

27 J. Borges-González, C. J. Kousseff and C. B. Nielsen, *J. Mater. Chem. C*, 2019, **7**, 1111–1130.

28 P. Lin and F. Yan, *Adv. Mater.*, 2012, **24**, 34–51.

29 G. N. Wei, J. L. Zhang, C. Jia, W. Z. Fan and L. R. Lin, *Spectrochim. Acta, Part A*, 2014, **128**, 168–175.

30 J. J. Ritter and G. H. Schmitz, *J. Am. Chem. Soc.*, 1929, **51**, 1587–1589.

31 C. Shang, Y. Cao, Z. Shao, C. Sun and Y. Li, *Spectrochim. Acta, Part A*, 2022, **267**, 120496.

32 N. Zink-Lorre, S. Seetharaman, D. Gutiérrez-Moreno, F. Fernández-Lázaro, P. A. Karr and F. D'Souza, *Chem. – Eur. J.*, 2021, **27**, 14996–15005.

33 F. A. S. Chipem, A. Mishra and G. Krishnamoorthy, *Phys. Chem. Chem. Phys.*, 2012, **14**, 8775–8790.

34 A. Sheehan, I. A. Okkelman, G. Groslambert, C. Bucher, R. I. Dmitriev and M. A. Filatov, *Chem. – Eur. J.*, 2025, **31**, e202404188.

35 D. Rajput, G. Rawat, P. Sorout, S. Kanvah and A. Mondal, *J. Phys. Chem. B*, 2024, **128**, 12559–12570.

36 M. Hecht and F. Wü, *Acc. Chem. Res.*, 2021, **54**, 642–653.

37 H. Piwoński, S. Nozue, H. Fujita, T. Michinobu and S. Habuchi, *Nano Lett.*, 2021, **21**, 2840–2847.

38 J. Wu, W. Liu, J. Ge, H. Zhang and P. Wang, *Chem. Soc. Rev.*, 2011, **40**, 3483–3495.

39 N. J. Britto, M. Panneerselvam, M. D. Kumar, A. Kathiravan and M. Jaccob, *J. Chem. Inf. Model.*, 2021, **61**, 1825–1839.

40 J. Seo, S. Kim and S. Y. Park, *J. Am. Chem. Soc.*, 2004, **126**, 11154–11155.

41 J. Wan, A. Ferreira, W. Xia, C. H. Chow, K. Takechi, P. V. Kamat, G. Jones II and V. I. Vullev, *J. Photochem. Photobiol., A*, 2008, **197**, 364–374.

42 A. Khasbaatar, Z. Xu, J. H. Lee, G. Campillo-Alvarado, C. Hwang, B. N. Onusaitis and Y. Diao, *Chem. Rev.*, 2023, **123**, 8395–8487.

43 CCDC 2480993: Experimental Crystal Structure Determination, 2025, DOI: **10.5517/ccdc.csd.cc2p8p1q**.